



# ENERGETIC NEUTRAL HYDROGEN OBSERVATIONS DEMONSTRATE THAT *VOYAGER 1* IS NOT OBSERVING THE EXTRAORDINARILY STRONG INTERSTELLAR MAGNETIC FIELD

G. GLOECKLER AND L. A. FISK

Department of Climate and Space Sciences and Engineering, University of Michigan, Ann Arbor, MI 48109, USA; [gglo@umich.edu](mailto:gglo@umich.edu)

Received 2016 August 4; revised 2016 October 10; accepted 2016 October 12; published 2016 December 21

## ABSTRACT

It is generally believed that *Voyager 1* (*VI*) is now in interstellar space, having crossed the heliopause at a heliocentric distance of 121.58 au in late August of 2012. Here we use recently published spectra of energetic neutral hydrogen, and the magnetic field and energetic particles directly measured by *VI* to find the average pressure in the inner heliosheath (termination shock to 122 au). This pressure turns out to be surprisingly large,  $(3.57 \pm 0.71) \times 10^{-12}$  dyn cm<sup>-2</sup>, and is completely dominated by pressures of pickup ions (PUIs), created in the inner heliosheath, and their suprathermal tails (43%), and PUIs and their tails that are produced upstream of the termination shock and enter the heliosheath (46%). We compute the total particle pressure in the outer heliosheath near the heliopause from distribution functions of the interstellar plasma and locally created PUIs using profiles of proton density, proton temperature, and neutral hydrogen density from model 2 in Zank et al., and find it to be at most  $7.7 \times 10^{-13}$  dyn cm<sup>-2</sup>. Balancing pressure across the heliopause, thus requires an unusually large magnetic pressure ( $2.8 \times 10^{-12}$  dyn cm<sup>-2</sup>). The resulting strength and  $1\sigma$  uncertainty of the draped magnetic field in the outer heliosheath near the heliopause is  $0.839 \pm 0.106$  nT. The  $3\sigma$  lower limit field strength (0.52 nT) is greater than the field of  $\sim 0.43 \pm 0.02$  nT measured by *VI*, implying that there is less than 1% probability that *VI* is measuring the interstellar draped field.

*Key words:* ISM: magnetic fields – Sun: heliosphere

## 1. INTRODUCTION

At each point of the surface of the heliopause the total pressure just inside must be equal to that just outside the heliopause, which separates the solar wind and solar magnetic field from the local interstellar field and plasma. In the inner heliosheath (between the termination shock and the heliopause), the distribution between the thermal and ram pressures of solar wind and pickup ions (PUIs) and magnetic pressure will vary with heliocentric distance. However, the sum of all these pressures at any distance must be the same throughout the entire inner heliosheath. In particular, the total pressure in the inner heliosheath at the heliopause must thus be the same as the total average pressure of the entire inner heliosheath.

Here we use recent observations (Galli et al. 2016) and the requirement of pressure balance across the heliopause, alleged to be at 122 au, to determine the magnetic field strength in the presumed outer heliosheath (perturbed interstellar space just beyond the heliopause) where *VI*, currently at  $\sim 135$  au, is assumed to be located. We find that the  $3\sigma$  lower limit is greater than the field strength currently measured by *VI* (Burlaga & Ness 2014), and conclude that *VI* has not yet crossed the heliopause, but remains in the heliosphere. In other words, it is extremely unlikely that *VI* is in local interstellar space.

## 2. METHOD

The average total pressure of the inner heliosheath is the sum of (a) the average magnetic pressure, (b) the average thermal pressures of solar wind ions and electrons, (c) the average ram pressure of solar wind ions (the ram pressure due to electrons is negligible), (d) the average thermal pressures of local and transmitted PUIs and their suprathermal tails, and (e) the average ram pressures of PUIs and their tails. These pressures, as well as the number densities,  $n$ , are computed using

Equation (1):

$$n = 4\pi \int_0^\infty f(v)v^2 dv; \quad P_{\text{th}} = \frac{4\pi m_p}{3} \int_0^\infty f(v)v^4 dv;$$

$$P_{\text{ram}} = \rho U_r^2; \quad P_{\text{mag}} = \frac{B^2}{8\pi},$$
(1)

where  $f(v)$  is the phase space density (psd) as a function of  $v$ , the particle speed in the solar wind or interstellar plasma reference frame,  $m_p$  is the proton mass,  $\rho$  the mass density, and  $U_r$  the radial component of the bulk speed of the solar wind or interstellar plasma.

In order to compute particle pressures we need to know the distribution functions,  $f_{j,k}(v)$ , for each major particle population, where  $j$  designates the charged particle's atomic mass (e.g.,  $j = 1$  for protons,  $j = 4$  for He, etc.) and  $k$  refers to one of the three major particle populations in the inner heliosheath (solar wind, transmitted PUIs (Gloeckler et al. 1997), and locally created PUIs) or the two most dominant particle populations (interstellar thermal plasma and locally created PUIs) in the outer heliosheath, where *VI* now presumably resides. Above  $\sim 40$  keV ( $2.8 \times 10^8$  cm s<sup>-1</sup>) *VI* measures the distribution functions (Krimigis et al. 2013), and above  $\sim 8.8 \times 10^8$  cm s<sup>-1</sup> it measures the composition (Krimigis et al. 2013) directly, and partial pressures above these high speeds are readily computed. Unfortunately, no direct particle measurements from *VI* are available below 40 keV. Therefore, we use the measured time-averaged velocity distribution function (psd versus particle speed,  $v_r$ ) of energetic neutral hydrogen (ENH) measured by *IBEX* (Galli et al. 2016), *Cassini* (Dialynas et al. 2013), and *SOHO* (Czechowski et al. 2008), shown as filled circles in Figure 1, to determine the proton velocity distributions  $f_{1,k}(v)$  in the inner heliosheath for speeds below  $2.8 \times 10^8$  cm s<sup>-1</sup>, where most of the total particle

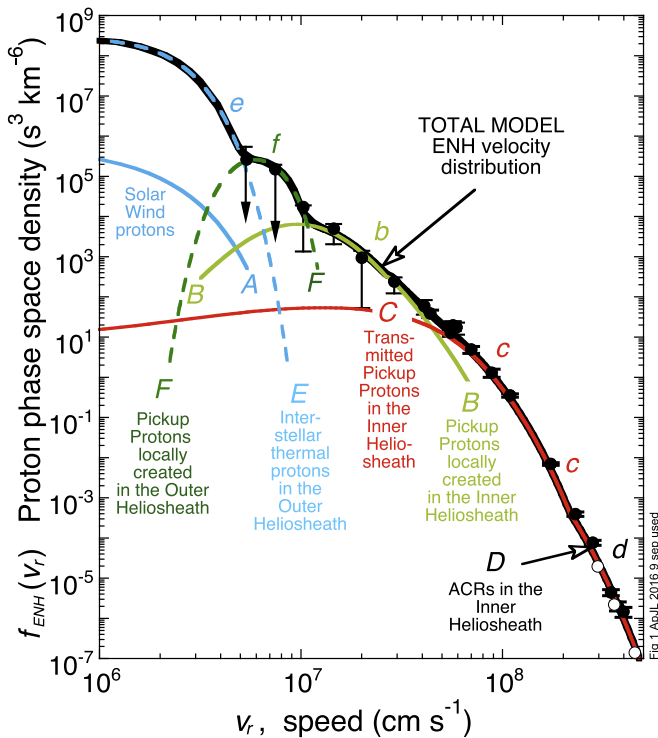


**Figure 1.** Time-averaged phase space density of energetic neutral hydrogen (ENH),  $f_{\text{ENH}}(v_r)$ , measured by *IBEX* (Galli et al. 2016) from  $\sim 5 \times 10^6$  to  $\sim 10^8$   $\text{cm s}^{-1}$ , *Cassini* (Dialynas et al. 2013) from  $\sim 1.1 \times 10^8$  to  $\sim 3.1 \times 10^8$   $\text{cm s}^{-1}$ , and *SOHO* (Czechowski et al. 2008) from  $\sim 3.1 \times 10^8$  to  $\sim 4.4 \times 10^8$   $\text{cm s}^{-1}$  (filled circles), vs. the radial component of the speed,  $v_r$ , of the hydrogen atoms. The sum of the five labeled ENH psd spectra of particle populations in the inner heliosheath and the outer heliosheath (curves A, B, C, D, and F) yields the total spectrum (bold curve) of ENH below  $\sim 4.4 \times 10^8$   $\text{cm s}^{-1}$  from the emission region (inner and outer heliosheaths) where this ENH is created. Open circles are the low end of the anomalous cosmic-ray (ACR) ENH spectrum derived from the proton spectrum directly measured (Krimigis et al. 2013) by *VI* in the inner heliosheath. In the text we describe how the five spectra were computed. Curve C is the velocity distribution of ENH created by transmitted pickup protons. The population of transmitted pickup ions (Gloeckler et al. 1997) is created in the supersonic solar wind upstream of the termination shock (TS), and convected with the solar wind across the TS. As they cross the TS, transmitted pickup ions are compressed and heated. Convected through the highly turbulent (Burlaga & Ness 2014) inner heliosheath, common spectrum (Fisk & Gloeckler 2014) ACR suprathermal tails develop on these pickup ion distributions.

pressure resides. In the caption to Figure 1 we describe in more detail the five particle populations that create the ENH particles.

We begin by computing the distribution functions of protons  $f_{1,k}(v)$  using Equation (2):

$$\begin{aligned}
 f_{1,k}(v) = & f_0 \exp\left(-\left(\frac{v_{\text{low}}}{v}\right)^{\alpha_{\text{low}}}\right) \left(1 + \frac{1}{\kappa} \left(\frac{v}{v_{\text{th}}}\right)^2\right)^{-\kappa} \\
 & \times \exp\left(-\left(\frac{v}{v_0}\right)^{100}\right) + f_{\text{tail}} \exp\left(-\left(\frac{v_0}{v}\right)^{100}\right) \left(\frac{v}{v_0}\right)^{-5} \\
 & \times \exp\left(-\left(\frac{v}{v_{\text{high}}}\right)^{\alpha_{\text{high}}}\right).
 \end{aligned}
 \tag{2}$$

Representative values of parameters used in Equation (2) are listed in rows *a* through *i*, columns 3–5 and 6 and 7 in Table 1,

and the respective ENH spectra are shown as curves A through F in Figure 1.

Previously, distribution functions observed (Fisk & Gloeckler 2014) at 1 au with *ACE*, and distribution functions of transmitted PUIs measured (Gloeckler et al. 1997) with *Ulysses* at  $\sim 5$  au, have been fit using Equation (2).

Next, we convert the proton distributions,  $f_{1,k}(v)$ , to the respective  $f_{\text{ENH},k}(v_r)$ , the ENH phase space densities, using Equation (3):

$$f_{\text{ENH},k}(v_r) = n(\text{HI})L\sigma(v_{\text{rel}})f_{1,k}(v_r - U_r),
 \tag{3}$$

which requires values for the neutral hydrogen gas density,  $n(\text{HI})$  for the radial width  $L$  of the respective emission regions ( $\sim 92$ – $122$  au for the inner heliosheath), for the H–p charge-exchange cross section  $\sigma(v_{\text{rel}})$  (Lindsay & Stebbings 2005), which depends on  $v_{\text{rel}}$ , the relative speed between the neutral gas and protons, and finally for  $U_r$ , the radial component of the bulk speed of the solar wind in the inner heliosheath, or of the plasma in the outer heliosheath. The values and errors we use for  $n(\text{HI})$  in the inner heliosheath are given in row 3, column 2 of Table 2,  $L$  is  $30 \pm 2$  au in the inner heliosheath, and the values for  $U_r$  in the inner heliosheath are taken from row 2, column 2 of Table 3.

The observed ENH spectrum (filled circles of Figure 1) must be matched by the sum (heavy solid curve) of the three spectra (curves B and C) that make the dominant contribution to the total observed ENH spectrum above  $5 \times 10^6$   $\text{cm s}^{-1}$  in two different velocity intervals (*b* and *c*). We assume that the solar wind spectrum in the inner heliosheath traversed by *VI* is the same as that measured by *Voyager 2* (Richardson 2016), in which case the solar wind (curve A) makes a negligible contribution to the measured total ENH spectrum. Next, we vary parameter values in Equation (2) for each of the two dominant populations, curves B and C in the inner heliosheath, to obtain the best fit (minimum reduced  $\chi^2$ ) to the observed ENH spectrum above  $\sim 1.2 \times 10^7$   $\text{cm s}^{-1}$ . The final set of parameters that gave the minimum reduced  $\chi^2 = 0.955$  is listed in rows *a* through *i* in Table 1. For the anomalous cosmic-ray (ACR) population (McDonald et al. 1974) (curve D) the parameters in column 6 of Table 1 are obtained from best fits to the proton spectrum directly measured (Krimigis et al. 2013) above 40 keV.

We use the three-parent proton velocity distribution,  $f_{1,k}(v)$ , in the ENA emission regions that together give the best fit to the observed ENH spectrum (filled circles in Figure 1) above  $1.2 \times 10^7$   $\text{cm s}^{-1}$ , the proton spectrum (Krimigis et al. 2013) of ACRs and the magnetic field strength (Burlaga & Ness 2014) in the inner heliosheath, both directly measured by *VI*, as well as the maxwellian solar wind proton spectrum observed by *Voyager 2* (Richardson 2016), assumed for the inner heliosheath traversed by *VI*, and we find the total average pressure in the inner heliosheath,  $P_{\text{IH}} = (3.57 \pm 0.71) \times 10^{-12}$   $\text{dyn cm}^{-2}$ , which is the sum of magnetic pressure and total particle pressure; the latter in turn is the sum of thermal and ram pressures of protons, heavy particles, and electrons. We used the standard procedure for propagation of errors to compute  $1\sigma$  errors of the total average pressures, taking into account that some of the uncertainties are correlated.

The total particle pressure in the outer heliosheath is the sum of (1) the thermal and (2) the ram pressures of (a) the interstellar plasma and (b) locally created PUIs. Few direct

**Table 1**  
Density, Thermal Pressure, Ram Pressure, and Parameter Values for Distribution Functions of Listed Populations in the Inner Heliosheath and the Outer Heliosheath near the Heliopause

Parameter	Inner Heliosheath $\sim 92\text{--}122$ au ( $L = 30 \pm 2$ au)				Outer Heliosheath near Heliopause 122 au [135 au]	
	(A) Solar Wind Ions <sup>a,b</sup>	(B) Locally Created Pickup Ions <sup>a</sup>	(C) Transmitted Pickup Ions <sup>a</sup>	(D) ACRs <sup>c</sup>	(E) Interstellar Thermal Ions <sup>a,b</sup>	(F) Locally Created Pickup Ions <sup>a</sup>
<i>a</i> Proton density (cm <sup>-3</sup> ) <sup>d</sup>	0.0019 <sup>e</sup>	0.0080	0.000362	$4.1 \times 10^{-7}$	0.09 [0.097] <sup>f</sup>	0.00083 [0.0012]
<i>b</i> $v_{\text{low}}$ (cm s <sup>-1</sup> )	0	$5.0 \times 10^7$	$1.0 \times 10^7$	...	0 [0]	$9.0 [9.0] \times 10^5$
<i>c</i> $\alpha_{\text{low}}$	0	1.17	1.0	...	0 [0]	2 [2]
<i>d</i> $v_{\text{th}}$ (cm s <sup>-1</sup> ) <sup>e</sup>	$2.92 \times 10^6$	$4.2 \times 10^6$	$4.0 \times 10^7$	...	$2.07 [2.01] \times 10^6$	$2.6 \times 10^6$
<i>e</i> $\kappa$	1000	100	6.01	...	1000 [1000]	4 [4]
<i>f</i> $v_0$ (cm s <sup>-1</sup> )	$10^{10}$	$1.35 \times 10^7$	$2.2 \times 10^8$	...	$10^{10} [10^{10}]$	$10^{10} [10^{10}]$
<i>g</i> $f_{\text{tail}}$ (s <sup>3</sup> km <sup>-6</sup> )	0	$2.0 \times 10^4$	0.03	...	0 [0]	0 [0]
<i>h</i> $v_{\text{high}}$ (cm s <sup>-1</sup> )	$10^8$	$5.0 \times 10^7$	$4 \times 10^9$	...	$10^{10} [10^{10}]$	$10^{10} [10^{10}]$
<i>i</i> $\alpha_{\text{high}}$	1.8	1.8	1.2	...	1.8 [1.8]	1.8 [1.8]
<i>j</i> Proton thermal pressure <sup>d,g</sup>	$1.54 \times 10^{-14}$	$8.94 \times 10^{-13}$	$1.06 \times 10^{-12}$	$1.51 \times 10^{-13}$	$3.23 [3.27] \times 10^{-14}$	$2.29 [3.35] \times 10^{-14}$
<i>k</i> Proton ram pressure <sup>d,g</sup>	$3.86 \times 10^{-14}$	$1.55 \times 10^{-13}$	$7 \times 10^{-15}$	$\sim 0$	$\sim 0 [6.60 \times 10^{-15}]$	$\sim 0 [8.25 \times 10^{-17}]$
<i>l</i> Ion and plasma electron thermal pressure <sup>d,g,h</sup>	$(3.49 \pm 0.61) \times 10^{-14}$	$(1.38 \pm 0.24) \times 10^{-12}$	$(1.64 \pm 0.28) \times 10^{-12}$	$(2.33 \pm 0.54) \times 10^{-13}$	$7.31 \times 10^{-13} [7.40 \times 10^{-13}]$	$3.55 \times 10^{-14} [5.18 \times 10^{-14}]$
<i>m</i> Ion ram pressure <sup>d,g,h</sup>	$(5.58 \pm 1.87) \times 10^{-14}$	$(1.75 \pm 0.59) \times 10^{-13}$	$(7.93 \pm 0.26) \times 10^{-15}$	$\sim 0$	$\sim 0 [9.55 \times 10^{-15}]$	$\sim 0 [9.36 \times 10^{-17}]$
<i>o</i> Magnetic pressure <sup>g</sup>	$(5.83 \pm 1.93)^k \times 10^{-14}$	...	...	...	$(2.80 [2.77] \pm 0.57)^h \times 10^{-12}$	...
<i>q</i> Magnetic field strength (nT)	$0.121 \pm 0.02^k$	...	...	...	$0.839 \pm 0.088^l [0.834 \pm 0.088]^l$	...

**Notes.**

<sup>a</sup> Use Equation (2) with parameter listed in rows *a* through *i*.

<sup>b</sup> Computed from Equation (2) with large  $\kappa$  (maxwellian) and values of density and thermal speed measured by *Voyager 2*.

<sup>c</sup> ACR density and pressures were computed using the proton spectrum directly measured (Krimigis et al. 2013) above 40 keV, corrected for contributions from galactic cosmic rays above  $\sim 5$  MeV.

<sup>d</sup> Densities, thermal pressures, ram pressures, and magnetic pressures are computed using the first, second, third, and fourth equations, respectively, in Equation (1).

<sup>e</sup> *Voyager 2* solar wind measurements (Richardson 2016) in the inner heliosheath.

<sup>f</sup> Values in brackets at 135 au.

<sup>g</sup> All pressures in units of dyn cm<sup>-2</sup>.

<sup>h</sup> Includes contributions from protons, electrons, and heavy ions for the populations of solar wind and interstellar thermal ions (columns 5 and 8), and protons as well as heavy ions for pickup ions and ACRs (columns 3, 4, 6, and 7). Since the composition (Ogilvie et al. 1989) of the solar wind is well known, as is the composition of transmitted pickup ions (Gloeckler et al. 2001) and ACRs (Krimigis et al. 2013), the total particle pressures are readily computed. For locally accelerated pickup ions (columns 4 and 7) we use solar wind abundances (Ogilvie et al. 1989).

<sup>k</sup> Average magnetic field strength measured (Burlaga & Ness 2014, 2016) by *V1* in the inner heliosheath. Magnetic pressure was calculated from the measured field strength using the fourth equation of Equation (1).

<sup>l</sup> Value and  $1\sigma$  error of magnetic pressure or field strength in the outer heliosheath derived from pressure balance.

**Table 2**Values and  $1\sigma$  Errors of Key Parameters in the Inner Heliosheath, and Angles between the *Voyager 1* Direction through the Heliosheath and Interstellar Flow Vector

Local Interstellar Cloud (LIC) Parameter	Mean and Standard Error <sup>a</sup>	Value 1 and $1\sigma$ Error	Value 2 and $1\sigma$ Error	Value 3 and $1\sigma$ Error	Value 4 and $1\sigma$ Error
Flow speed, $V_o$ (km s <sup>-1</sup> )	26.12 ± 0.27	25.4 ± 1.1 <sup>b</sup>	26.7 ± 0.5 <sup>c</sup>	26.08 ± 0.21 <sup>d</sup>	26.3 ± 0.4 <sup>e</sup>
Neutral hydrogen density, $n(\text{HI})$ (cm <sup>-3</sup> )	0.125 ± 0.016	0.09 ± 0.02 <sup>f</sup>	0.115 ± 0.025 <sup>g</sup>	0.165 ± 0.035 <sup>h</sup>	0.13 ± 0.04 <sup>i</sup>
Temperature, $T_0$ (K)	7427 ± 423	8000 ± 1300 <sup>b</sup>	8150 ± 390 <sup>c</sup>	7260 ± 270 <sup>d</sup>	6300 ± 340 <sup>e</sup>
Thermal speed (cm s <sup>-1</sup> )	(1.11 ± 0.26) × 10 <sup>6</sup>	...	...	...	...
Polar angle of <i>VI</i> relative to flow, $\alpha^j$	~30°	...	...	...	...
Azimuthal angle of <i>VI</i> relative to flow, $\beta^j$	~5°	...	...	...	...

**Notes.**<sup>a</sup> Mean values and standard error of respective parameters of columns 3–6.<sup>b</sup> Schwadron et al. (2015).<sup>c</sup> Bzowski et al. (2015).<sup>d</sup> Wood et al. (2015).<sup>e</sup> Witte (2004).<sup>f</sup> Richardson et al. (2008).<sup>g</sup> Gloeckler et al. (1997).<sup>h</sup> Quemerais et al. (1994).<sup>i</sup> Czechowski et al. (2008).<sup>j</sup> Parameters required to compute the relative speed,  $v_{\text{rel}}$ , in Equation (3), where  $v_{\text{rel}} = \sqrt{(V_0 \cos \alpha \cos \beta - v_r - U_r)^2 + (V_0 \cos \alpha \sin \beta - U_l)^2 + (V_0 \sin \alpha - U_n)^2}$ .**Table 3**Mean Values and Errors of Solar Wind Parameters and Magnetic Field Strength in the Inner Heliosheath (94–122 au) and Outer Heliosheath (122–135 au) Measured by *Voyager 1* and *Voyager 2*

Parameter	~94 to ~122 au	~122 to ~135 au
Mean radial component of flow speed, $U_r$ (km s <sup>-1</sup> )	34.0 ± 6.9 <sup>a</sup>	...
Number density of protons, $n_p$ (cm <sup>-3</sup> )	0.0019 ± 0.0007 <sup>b</sup>	0.085 ± .01 <sup>c</sup> 0.0935 <sup>d</sup>
Thermal speed, $v_{\text{th}}$ (km s <sup>-1</sup> )	29.2 ± 0.07 <sup>b</sup>	20.5 <sup>d</sup>

**Notes.**<sup>a</sup> Decker et al. (2012).<sup>b</sup> *Voyager 2* solar wind measurements (Richardson 2016) in the inner heliosheath.<sup>c</sup> Gurnett et al. (2013).<sup>d</sup> Model 2 in Figure 4 in Zank et al. (2013).

measurements of interstellar parameters are available, let alone their variations with heliocentric distance along the *VI* trajectory. Here we use radial profiles of the number density of interstellar plasma protons and the temperature from model 2 in Figure 4 of Zank et al. (2013). The reason for choosing their model 2 is because the value for the proton density in the outer heliosheath near the heliopause (0.09 cm<sup>-3</sup>) agrees well with the value measured by the Plasma Wave System instrument on *VI* in the outer heliosheath, where *VI* is now presumably located (Gurnett et al. 2013). The parameters we use to characterize the outer heliosheath plasma at 122 au and [in brackets] at 135 au are listed in column 7, rows *a* through *i* of Table 1. Note that we model the plasma psd distribution as a maxwellian (very large  $\kappa$  in Equation (2)), with no suprathermal tail. This type of distribution is quite reasonable because the measured magnetic field (Burlaga & Ness 2014) in that

region is so exceptionally smooth (nonturbulent). In the absence of turbulence, maxwellian distributions without tails are generally observed (Fisk & Gloeckler 2014).

Pickup ions created beyond the heliopause also contribute to the balancing pressure in the outer heliosheath. We compute the density profile of these PUIs using Equation (5) in Vasyliunas & Siscoe (1976), with the radial profiles of neutral hydrogen and proton number densities from model 2 in Figure 8 and Figure 4, respectively, of Zank et al. (2013), and the H–p cross section of Lindsay & Stebbings (2005). The parameters for the psd distribution of these PUIs are listed in column 8, rows *a* through *i* of Table 1. Again, for reasons discussed above we assume that these PUI distributions will also have no significant tails.

Interstellar neutrals will charge-exchange with thermal protons and pickup protons in the outer heliosheath to produce ENHs primarily below  $\sim 1.2 \times 10^7$  cm s<sup>-1</sup>. Integrating the derived radial profiles of these velocity distributions in the outer heliosheath, we compute the ENH spectrum and correct for the survival probability (Fuselier et al. 2012) of these low-energy neutrals from their point of origin to 100 au. The parameters listed in column 8, rows *b* through *i* of Table 1 provide the best fits to the *IBEX* ENH spectrum below  $1.2 \times 10^7$  cm s<sup>-1</sup>.

While we have argued above that suprathermal tails on plasma velocity distributions would most likely not be produced in the outer heliosheath where we assume *VI* is now located, it is quite plausible that some inner heliosheath ACRs will escape into the outer heliosheath. The density of these interstellar ACR suprathermal tails would have to be at least a factor of 1000 less than in the inner heliosheath since otherwise an upturn in the spectrum of Galactic cosmic rays currently measured by *VI* below 5 MeV would be observed. Indeed, suprathermal tails have been proposed by Cummings et al. (2016) as one possibility to explain the discrepancy by a

factor of 11–12 in the ionization rates of atomic hydrogen in the local interstellar medium using, on the one hand, astrochemistry methods, and on the other, the energy spectra of Galactic cosmic rays. To match the ionization rate obtained by astrochemistry methods, they find that the density and pressure in their suprathermal tails must be  $\sim 8 \times 10^{-7} \text{ cm}^{-3}$  and  $\sim 10^{-15} \text{ dyn cm}^{-2}$ , respectively. This pressure has also been included in our calculations of balancing pressure.

Pressure balance across the heliopause requires that the total pressure in the outer heliosheath,  $P_{\text{OH}}$ , must be the same as the total pressure in the inner heliosheath,  $P_{\text{IH}}$ . To achieve this pressure balance at the presumed heliopause at 122 au requires that the unknown magnetic pressure in the outer heliosheath is given by  $P_{\text{OH,mag}} = P_{\text{IH}} - P_{\text{OH,particle}}$ , where the last term is the total particle pressure in the outer heliosheath. That is,  $P_{\text{OH,mag}} = P_{\text{IH}} - P_{\text{OH,particle}} = 3.57 \times 10^{-12} - 7.68 \times 10^{-13} = 2.8 \times 10^{-12} \text{ dyn cm}^{-2}$ . From the fourth equation in Equation (1), the value and  $1\sigma$  uncertainty of the strength of the draped magnetic field in the outer heliosheath at the heliopause (122 au) is  $0.839 \pm 0.106 \text{ nT}$ . A similar calculation shows that the strength of the draped field at 135 au, where *VI* is now located, is slightly less,  $0.834 \pm 0.106 \text{ nT}$ .

### 3. CONCLUSIONS

The  $3\sigma$  lower limit of the calculated magnetic field (0.521 nT) is still larger than the field strength of  $0.43 \pm 0.01 \text{ nT}$  measured by *VI* from 121.58 to 123 au (Burlaga & Ness 2014), implying that there is a 99% certainty that the weak magnetic field strength currently measured by *VI* is, in fact, *not* that of the interstellar field in the outer heliosheath. It is thus extremely unlikely that *VI* crossed the heliopause and entered the outer heliosheath in late August of 2012. Rather, it must be concluded that *VI* is currently not in the outer heliosheath, nor in the local interstellar medium. *Voyager 1*, however, is certainly in a most unusual region of the heliosphere, a region never before explored. The plasma properties of this unusual region of the inner heliosheath are discussed in Gloeckler & Fisk (2014).

The measured averaged ENH differential intensity, together with the in situ measurements of  $>40 \text{ keV}$  particles, show clearly that PUIs, both transmitted and locally created, and their suprathermal tails (ACRs) account for 96% of the total pressure in the inner heliosheath and thus completely dominate the dynamics of the heliosphere. It is therefore essential to develop numerical models of the heliosphere that include not only the

thermal populations that carry the mass but also those particle populations that carry the pressure.

We thank E. Möbius, Alan Cummings, and G. Zank for their useful comments. Some of the data used in our analysis are publicly available at <http://omniweb.gsfc.nasa.gov/coho/form/voyager1.html> and [http://web.mit.edu/afs/athena/org/s/space/www/voyager/voyager\\_data/voyager\\_data.html](http://web.mit.edu/afs/athena/org/s/space/www/voyager/voyager_data/voyager_data.html). This work was supported in part by NASA Grant NNX10AF23G.

### REFERENCES

- Burlaga, L. F., & Ness, N. F. 2014, *ApJL*, 795, L19  
 Burlaga, L. F., & Ness, N. F. 2016, GSFC website for Voyager data: <http://omniweb.gsfc.nasa.gov/coho/form/voyager1.html>  
 Bzowski, M., Swaczyna, P., Kubiak, M. A., et al. 2015, *ApJS*, 220, 28  
 Cummings, A. C., Stone, E. C., Heikkilä, B. C., et al. 2016, *ApJ*, 831, 18  
 Czechowski, A., Hilchenbach, M., Hsieh, K. C., Grzedzielski, S., & Kóta, J. 2008, *A&A*, 487, 329  
 Decker, R. B., Krimigis, S. M., Roelof, E. C., & Hill, M. E. 2012, *Natur*, 489, 124  
 Dialynas, K., Krimigis, S. M., Mitchell, D. G., Roelof, E. C., & Decker, R. B. 2013, *ApJ*, 778, 40  
 Fisk, L. A., & Gloeckler, G. 2014, *JGRA*, 119, 8733  
 Fuselier, S. A., Allegrini, F., Bzowski, M., et al. 2012, *ApJ*, 754, 14  
 Galli, A., Wurz, P., Schwadron, N. A., et al. 2016, *ApJ*, 821, 107  
 Gloeckler, G., & Fisk, L. A. 2014, in ASP Conf. Ser. 484, Outstanding Problems in Heliophysics: From Coronal Heating to the Edge of the Heliosphere, ed. Q. Hu & G. P. Zank (San Francisco, CA: ASP), 55  
 Gloeckler, G., Fisk, L. A., & Geiss, J. 1997, *Natur*, 386, 374  
 Gloeckler, G., Geiss, J., & Fisk, L. A. 2001, in The Heliosphere near Solar Minimum: the Ulysses Perspectives, ed. A. Balogh et al. (London: Springer-Praxis), 287  
 Gumett, D. A., Kurth, W. S., Burlaga, L. F., & Ness, N. F. 2013, *Sci*, 341, 1481  
 Krimigis, S. M., Decker, R. B., Roelof, E. D., et al. 2013, *Sci*, 341, 144  
 Lindsay, B. G., & Stebbings, R. F. 2005, *JGR*, 110, A12213  
 McDonald, F. B., Teegarden, B. J., Trainor, J. H., & Webber, W. R. 1974, *ApJL*, 187, L105  
 Ogilvie, K. W., Coplan, M. A., Bochsler, P., & Geiss, J. 1989, *SoPh*, 124, 167  
 Quemerais, E., Bertaux, J.-L., Sandel, B. R., & Lallement, R. 1994, *A&A*, 290, 941  
 Richardson, J. D. 2016, MIT website for Voyager 2 Solar Wind data: [http://web.mit.edu/afs/athena/org/s/space/www/voyager/voyager\\_data/voyager\\_data.html](http://web.mit.edu/afs/athena/org/s/space/www/voyager/voyager_data/voyager_data.html)  
 Richardson, J. D., Liu, Y., Wang, C., & McComas, D. J. 2008, *A&A*, 491, 1  
 Schwadron, N. A., Möbius, E., Leonard, T., et al. 2015, *ApJS*, 220, 25  
 Vasyliunas, V. M., & Siscoe, G. L. 1976, *JGR*, 81, 1247  
 Witte, M. 2004, *A&A*, 426, 835  
 Wood, B. E., Müller, H.-R., Bzowski, M., et al. 2015, *ApJS*, 220, 31  
 Zank, G. P., Heerikhuisen, J., Wood, B. E., et al. 2013, *ApJ*, 763, 20